Photon collisions with atoms and ions within an intermediate-energy *R*-matrix framework

M. P. Scott,* A. J. Kinnen, and M. W. McIntyre
School of Mathematics and Physics, Queen's University Belfast, Belfast BT7 1NN, United Kingdom
(Received 13 June 2012; published 12 September 2012)

Recent experimental advances in light technology necessitate the availability of sophisticated theoretical models which can incorporate an accurate treatment of double-electron continua. We describe here an intermediate-energy *R*-matrix approach to photoionization and photo-double-ionization and illustrate its feasibility by application to photoionization and photo-double-ionization of He and photodetachment and photo-double-detachment of H^-. Results are shown to be in excellent agreement with previous theoretical and experimental studies. This work is a key step in the development of a multipurpose *R*-matrix code for multiple-electron ejection.

DOI: 10.1103/PhysRevA.86.032707 PACS number(s): 03.65.Nk

I. INTRODUCTION

Recent advances in the field of attosecond science (see, e.g., Corkum and Krausz [1]) yield an enhanced insight into time-resolved dynamics of ultrafast laser-driven excitations of atoms and ions. In addition, the advancement of x-ray free-electron laser sources, such as the Linac Coherent Light Source at the SLAC National Accelerator Laboratory, is generating exciting new experimental data for inner-shell photoionization processes (see, e.g., Rohringer *et al.* [2]). In both areas, the light fields contain highly energetic photons with sufficient energy that absorption can lead to the excitation and/or emission of several electrons. A full interpretation of experimental results thus necessitates an understanding of multielectron dynamics, and two-electron dynamics in particular.

To complement the experimental advances in light technology, it is essential to have advanced theoretical models which incorporate an accurate treatment of double-electron continua, both within a time-dependent and time-independent framework. While the time-independent *R*-matrix method for photoionization has been in worldwide use for many years (see, e.g., Burke and Taylor [3]), it is only recently that an *ab initio* time-dependent *R*-matrix approach has been developed to facilitate the study of the interaction of ultrashort light fields with many-electron atoms and ions (Lysaght *et al.* [4], Moore *et al.* [5]). We now seek a suitable *R*-matrix–based approach to incorporate double-electron continua. Toward this end, we report here the development and implementation of an intermediate-energy *R*-matrix (IERM) approach to photoionization and photo-double-ionization, and investigate the suitability of this method by comparing results for photoionization and photo-double-ionization of He, and photodetachment and photo-double-detachment of H^-, with exisiting theoretical and experimental data.

The IERM approach for the accurate description of double-electron continua has already been proved highly successful in the study of electron collisions with one-electron systems [6–8]. The current work focuses on photon collisions with two-electron systems within a time-independent framework. This is an essential first step toward our ultimate goal of the development of many-electron, time-dependent and time-independent *R*-matrix codes, capable of accurate treatment of double-electron continua. Such codes will also be able to provide accurate data to assess the feasibility of planned experimental studies at leading-edge facilities.

The rest of this paper is organized as follows: In Sec. II we derive the IERM theory for photon collisions with two-electron atoms and ions, while in Secs. III and IV we present results for photoionization and photo-double-ionization of He and photodetachment and photo-double-detachment of H^-. Conclusions are drawn in Sec. V.

II. THEORY

The differential cross section for photoionization of a two-electron atom or ion with the ejection of the photoelectron in the direction $\hat{\mathbf{k}}$ is given, in the length approximation, by

$$\frac{d\sigma_L}{d\hat{\mathbf{k}}} = 8\pi^2\alpha a_0^2\omega|\langle\Psi_f^-(\hat{\mathbf{k}}) \mid \hat{\mathbf{e}}\cdot\mathbf{M} \mid \Psi_i\rangle|^2, \tag{1}$$

where

$$\mathbf{M} = \mathbf{r}_1 + \mathbf{r}_2. \tag{2}$$

Here α is the fine structure constant, a_0 is the Bohr radius of the hydrogen atom, and ω is the incident photon energy in atomic units, while $\hat{\mathbf{e}}$ is the polarization vector. The integration in Eq. (1) is over the spatial coordinates of the two electrons. The initial- and final-state wave functions Ψ_i and $\Psi_f^-(\hat{\mathbf{k}})$ are solutions of the Schrödinger equation

$$(H - E)\Psi = 0, \tag{3}$$

where H is the two-electron Hamiltonian operator:

$$H = \left(-\frac{1}{2}\nabla_1^2 - \frac{Z}{r_1}\right) + \left(-\frac{1}{2}\nabla_2^2 - \frac{Z}{r_2}\right) + \frac{1}{r_{12}}. \tag{4}$$

The initial state Ψ_i has total orbital angular momentum L_i, total spin angular momentum S_i and parity Π_i; the final two-electron state, consisting of the residual ion plus photoelectron, has corresponding quantum numbers L, S, and Π, respectively. The orbital angular momentum, spin angular momentum, and parity of the residual one-electron ion are L_f, S_f, and Π_f. The final-state wave function $\Psi_f^-(\hat{\mathbf{k}})$ satisfies the boundary condition corresponding to a plane wave in the direction $\hat{\mathbf{k}}$ incident on the residual ion, with ingoing waves in all open channels. Ψ_i and $\Psi_f^-(\hat{\mathbf{k}})$ are normalized so that

$$\langle\Psi_i \mid \Psi_i\rangle = 1 \tag{5}$$

*m.p.scott@qub.ac.uk

and

$$\langle \Psi_f^-(\hat{\mathbf{k}}) \mid \Psi_{f'}^-(\hat{\mathbf{k}}')\rangle = \delta_{ff'}\,\delta\left(\tfrac{1}{2}k^2 - \tfrac{1}{2}k'^2\right). \tag{6}$$

The total cross section for photoionization by unpolarized light can be obtained by integrating Eq. (1) over all photoelectron angles $\hat{\mathbf{k}}$ and averaging over all photon polarization directions. This gives the following expression for the total cross section:

$$\sigma = \frac{8\pi^2\alpha a_0^2\omega}{3(2L_i+1)}\sum_{\ell_f L}|\langle\Psi_f^-\|M\|\Psi_i\rangle|^2. \tag{7}$$

The summation in Eq. (7) is over all possible final-state orbital angular momenta L of the two-electron system permitted by dipole selection rules, and over ℓ_f the orbital angular momentum of the ejected photoelectron which can couple with the orbital angular momentum of the residual ion L_f to give L. We have introduced the reduced dipole matrix element in the summation on the right-hand side of Eq. (7) which, according to the Wigner-Eckart theorem, is given by

$$\langle\Psi_f^-\|M\|\Psi_i\rangle = \frac{(2L+1)^{\frac{1}{2}}}{C\left(L_i 1 L; M_{L_i}\mu M_L\right)}\langle\Psi_f^-|M^\mu|\Psi_i\rangle. \tag{8}$$

As in the application of R-matrix theory to other atomic collision processes, configuration space is divided into two regions using a sphere of radius $r = a$, centered on the target nucleus; r, in this application, is the relative radial coordinate of the photoelectron. In the internal region, both Ψ_i and Ψ_f^- are expanded in terms of appropriate sets of energy-independent, two-electron R-matrix basis functions $\{\Theta_k^{L_i S_i \Pi_i}(\mathbf{r}_1,\mathbf{r}_2)\}$ and $\{\Theta_k^{LS\Pi}(\mathbf{r}_1,\mathbf{r}_2)\}$ as follows:

$$\Psi_i = \sum_k A_{ki}\Theta_k^{L_i S_i \Pi_i}, \tag{9}$$

$$\Psi_f^- = \sum_k A_{kf}\Theta_k^{LS\Pi}. \tag{10}$$

The R-matrix basis sets $\{\Theta_k^{L_i S_i \Pi_i}(\mathbf{r}_1,\mathbf{r}_2)\}$ and $\{\Theta_k^{LS\Pi}(\mathbf{r}_1,\mathbf{r}_2)\}$ are constructed from two-electron functions $\chi_{n_1\ell_1 n_2\ell_2}(\mathbf{r}_1,\mathbf{r}_2)$:

$$\Theta_k^{L_i S_i \Pi_i} = \sum_{n_1'\ell_1' n_2'\ell_2'}\chi_{n_1'\ell_1' n_2'\ell_2'}^{L_i S_i \Pi_i}(\mathbf{r}_1,\mathbf{r}_2)\beta_{n_1'\ell_1' n_2'\ell_2' k}^{L_i S_i \Pi_i} \tag{11}$$

and

$$\Theta_k^{LS\Pi} = \sum_{n_1\ell_1 n_2\ell_2}\chi_{n_1\ell_1 n_2\ell_2}^{LS\Pi}(\mathbf{r}_1,\mathbf{r}_2)\beta_{n_1\ell_1 n_2\ell_2 k}^{LS\Pi}. \tag{12}$$

We note that

$$\begin{aligned}&\chi_{n_1\ell_1 n_2\ell_2}^{LS\Pi}(\mathbf{r}_1,\mathbf{r}_2)\\ &= \frac{1}{\sqrt{2}}\big\{r_1^{-1}r_2^{-1}u_{n_1\ell_1}(r_1)\,u_{n_2\ell_2}(r_2)\mathcal{Y}_{\ell_1\ell_2 L M_L}(\hat{\mathbf{r}}_1,\hat{\mathbf{r}}_2)\\ &\quad + (-)^{\ell_1+\ell_2+L+S}r_1^{-1}r_2^{-1}u_{n_1\ell_1}(r_2)\,u_{n_2\ell_2}(r_1)\\ &\quad \times \mathcal{Y}_{\ell_2\ell_1 L M_L}(\hat{\mathbf{r}}_1,\hat{\mathbf{r}}_2)\big\} \quad \text{if} \quad n_1\ell_1 \neq n_2\ell_2\end{aligned}$$

and

$$\begin{aligned}&\chi_{n\ell n\ell}^{LS\Pi}(\mathbf{r}_1,\mathbf{r}_2)\\ &= r_1^{-1}r_2^{-1}u_{n\ell}(r_1)\,u_{n\ell}(r_2)\mathcal{Y}_{\ell\ell L M_L}(\hat{\mathbf{r}}_1,\hat{\mathbf{r}}_1) \quad \text{if} \quad n_1\ell_1 = n_2\ell_2.\end{aligned} \tag{13}$$

In Eq. (13) the radial functions $u_{n\ell}(r)$ are solutions of the second-order differential equation

$$\left(\frac{d^2}{dr^2} - \frac{\ell(\ell+1)}{r^2} + \frac{2Z}{r} + k_{n\ell}^2\right)u_{n\ell}(r) = 0, \tag{14}$$

subject to the boundary conditions

$$u_{n\ell}(0) = 0, \quad \left(\frac{a}{u_{n\ell}}\right)\frac{du_{n\ell}}{dr}\bigg|_{r=a} = 0.$$

We choose the R-matrix boundary radius $r = a$ sufficiently large so that the radial functions of the physical states of interest of the residual ion are completely enveloped by this boundary and generated by Eq. (14). We also ensure that the initial-state wave function Ψ_i is completely enclosed within the interaction volume defined by $r = a$. The angular functions $\mathcal{Y}_{\ell_1\ell_2 L M_L}(\hat{\mathbf{r}}_1,\hat{\mathbf{r}}_2)$ are defined by

$$\begin{aligned}&\mathcal{Y}_{\ell_1\ell_2 L M_L}(\hat{\mathbf{r}}_1,\hat{\mathbf{r}}_2)\\ &= \sum_{m_{\ell_1},m_{\ell_2}} C\left(\ell_1\ell_2 L; m_{\ell_1}m_{\ell_2}M_L\right)Y_{\ell_1 m_{\ell_1}}(\hat{\mathbf{r}}_1)Y_{\ell_2 m_{\ell_2}}(\hat{\mathbf{r}}_2).\end{aligned} \tag{15}$$

The coefficients $\beta_{n_1\ell_1 n_2\ell_2 k}$ in Eqs. (11) and (12) are obtained by diagonalizing the appropriate two-electron Hamiltonian matrix. This ensures that the R-matrix basis functions $\{\Theta_k^{L_i S_i \Pi_i}(\mathbf{r}_1,\mathbf{r}_2)\}$ and $\{\Theta_k^{LS\Pi}(\mathbf{r}_1,\mathbf{r}_2)\}$ satisfy

$$\left\langle\Theta_k^{L_i S_i \Pi_i}(\mathbf{r}_1,\mathbf{r}_2)\middle|H\middle|\Theta_{k'}^{L_i S_i \Pi_i}(\mathbf{r}_1,\mathbf{r}_2)\right\rangle = \delta_{kk'}E_{ki} \tag{16}$$

and

$$\left\langle\Theta_k^{LS\Pi}(\mathbf{r}_1,\mathbf{r}_2)\middle|H\middle|\Theta_{k'}^{LS\Pi}(\mathbf{r}_1,\mathbf{r}_2)\right\rangle = \delta_{kk'}E_{kf}, \tag{17}$$

respectively.

We note that other bases could possibly have been considered to form the orbital set $\{u_{n\ell}\}$, e.g., B-splines have been used very successfully in a number of recent R-matrix calculations [9,10]. However, in this work we have retained the same one-electron basis as proposed by Burke *et al.* [6], since this basis is consistent with the one-electron basis used in the recently developed two-dimensional R-matrix propagator, 2DRMP [11], with which we intend to link for future many-electron atom and ion calculations. The basis generated by Eq. (14) is a flexible, orthogonal basis: By careful choice of the boundary radius we are able to generate the required physical states of the residual one-electron ion, while also being able to create a suitably dense pseudostate basis which can be used to discretize the ionic electron continuum in photo-double-ionization calculations.

Returning to Eqs. (9) and (10), the expansion coefficients A_{ki} and A_{kf} are given by (see, e.g., Burke and Taylor [3])

$$A_{ki} = \frac{1}{2a(E_{ki}-E_i)}\sum_j w_{jk}(a)\left(a\frac{dy_{ji}}{dr} - by_{ji}\right)_{r=a} \tag{18}$$

and

$$A_{kf} = \frac{1}{2a(E_{kf}-E_i-\omega)}\sum_j w_{jk}(a)\left(a\frac{dy_{jf}^-}{dr} - by_{jf}^-\right)_{r=a}, \tag{19}$$

where E_i is the energy of the initial state; $w_{jk}(a)$ are surface amplitudes, defined in terms of the radial functions $u_{n_1 l_1}(a)$ on the boundary of the internal region by

$$w_{jk}(a) = \sum_{n_1} \beta_{n_1 \ell_1 n_2 \ell_2 k} u_{n_1 \ell_1}(a), \quad j \equiv n_2 \ell_2 \ell_1. \tag{20}$$

We note that the surface amplitudes $w_{jk}(a)$ in Eqs. (18) and (19) are not the same, since Ψ_i and Ψ_f^- have different angular symmetries and a different set of surface amplitudes will be obtained for the initial- and final-state calculations. y_{ji} and y_{jf}^- describe the radial motion of the photoelectron in channel j in the initial and final states, respectively. These functions satisfy the equation

$$y_{jp}(a) = \sum_{t=1}^{n_{\rm chan}} R_{jt} \left(\frac{dy_{tp}}{dr} - b y_{tp} \right)_{r=a} \qquad j = 1, \ldots, n_{\rm chan}, \tag{21}$$

where p represents either i or f as appropriate and R_{jt} are elements of the multichannel R-matrix. $n_{\rm chan}$ is the total number of channels. Rewriting (21) in matrix notation we obtain

$$\mathbf{y}(a) = \mathbf{R} \times \left(a \frac{d\mathbf{y}_p}{dr} - b \mathbf{y}_p \right)_{r=a}. \tag{22}$$

Substituting Eq. (22) into Eqs. (18) and (19) yields the expressions

$$A_{ki} = \mathbf{G}_i \mathbf{W}_{ki}^T(a) \mathbf{R}_i^{-1} \mathbf{y}_i(a), \tag{23}$$

$$A_{kf} = \mathbf{G}_f \mathbf{W}_{kf}^T(a) \mathbf{R}_f^{-1} \mathbf{y}_f(a), \tag{24}$$

where we have introduced the diagonal matrices $\mathbf{G}_i$ and $\mathbf{G}_f$:

$$\mathbf{G}_i = \frac{1}{2a(E_{ki} - E_i)}, \tag{25}$$

$$\mathbf{G}_f = \frac{1}{2a(E_{kf} - E_i - \omega)}. \tag{26}$$

The $\mathbf{W}$ matrices are defined by Eq. (20).

We define matrices $\mathbf{V}_i$ and $\mathbf{V}_f$, whose columns consist of the β coefficients introduced in Eqs. (11) and (12), i.e.,

$$V_{i_{t'k}} = \beta_{t'k}^{L_i S_i \Pi_i}, \quad t' \equiv n_1' \ell_1' n_2' \ell_2' \tag{27}$$

and

$$V_{f_{tk}} = \beta_{tk}^{LS\Pi}, \quad t \equiv n_1 \ell_1 n_2 \ell_2. \tag{28}$$

Defining the reduced dipole matrix $\mathbf{M}$ by

$$\mathbf{M} = \langle \chi_{n_1 \ell_1 n_2 \ell_2}^{LS\Pi} \| M \| \chi_{n_1' \ell_1' n_2' \ell_2'}^{L_i S_i \Pi_i} \rangle, \tag{29}$$

it is possible to rewrite the expression for the photoionization cross section σ as

$$\sigma = \frac{8\pi^2 \alpha a_0^2 \omega}{3(2L_i + 1)} \sum_{\ell_f L} \left| \mathbf{y}_f^T \mathbf{R}_f^{-1} \mathbf{W}_f \mathbf{G}_f \mathbf{V}_f^T \mathbf{M} \mathbf{V}_i \mathbf{G}_i \mathbf{W}_i^T \mathbf{R}_i^{-1} \mathbf{y}_i \right|^2. \tag{30}$$

We will assume that the interaction volume is sufficiently large and our approximation sufficiently accurate so that the energy of the initial state E_i is extremely close to one of the eigenvalues $E_{k'i}$ in Eq. (16), and that the contribution to the initial-state wave function from closed channels in the external region, as represented by Eq. (21), can be neglected. The expression for A_{ki} then simplifies considerably to

$$A_{ki} = \begin{cases} 1 & \text{if} \quad k = k' \\ 0 & \text{otherwise.} \end{cases} \tag{31}$$

Equation (30) then reduces to

$$\sigma = \frac{8\pi^2 \alpha a_0^2 \omega}{3(2L_i + 1)} \sum_{\ell_f L} \left| \mathbf{y}_f^T \mathbf{R}_f^{-1} \mathbf{W}_f \mathbf{G}_f \mathbf{V}_f^T \mathbf{M} \mathbf{V}_{i_{k'}} \right|^2, \tag{32}$$

where $\mathbf{V}_{i_{k'}}$ is the eigenvector of the initial-state Hamiltonian matrix associated with the eigenvalue $E_{k'i}$. Provided that $E_{k'i}$ is sufficiently close to the experimental value for E_i, it is possible to improve our theoretical value for the initial-state energy by making a very small adjustment to the appropriate diagonal element of the Hamiltonian matrix, prior to diagonalization.

All entities in Eq. (32) are evaluated within the internal region except for $\mathbf{y}_f^T$, which is obtained by solving the scattering problem for the residual ion in the external region, and matching to the inner region solution on the boundary through the R-matrix, as illustrated by Eq. (22). One of the advantages of the R-matrix method is that the bulk of the computational work lies in the construction and diagonalization of the Hamiltonian matrix in the internal region which, being energy-independent, needs to be carried out only once for each partial wave. The energy dependence appears in the denominator of the R-matrix and in the evaluation of $\mathbf{y}_f^T$ in the external region, which are considerably less onerous. As such, it is relatively easy to calculate cross sections over a very fine energy mesh, once the inner region problem has been solved.

To test the above theory we have applied the IERM method for photoionization to photoionization and photo-double-ionization of He and photodetachment and photo-double-detachment of H^-. Details of these calculations are given in the next two sections.

III. PHOTOIONIZATION AND PHOTO-DOUBLE-IONIZATION OF He

A. Calculation

We first consider photoionization of the $^1S^e$ ground state of He with the emission of a single electron, focusing on the energy region between the $n = 2$ and $n = 3$ thresholds, due to the wealth of existing data with which to compare. As seen from Sec. II, the two-electron wave function for the ground state of He is described in terms of products of one-electron He^+ orbitals. Clearly, the He^+ $1s$ orbital and the He $1s$ orbital of the $1s^2\ ^1S^e$ ground state are significantly different. Hence, if we are to use the He^+ one-electron orbital basis, it is essential that this basis contains a sufficiently large number of pseudo-orbitals to correct for this. We have therefore chosen to use a one-electron orbital basis for the residual He^+ ion consisting of the physical He^+ orbitals $1s, 2s, 2p, 3s, 3p, 3d, 4s, 4p, 4d$, and $4f$, augmented by pseudo-orbitals $n = 5$ to $n = 38$, with angular momentum $\ell = 0, \ldots, 3$. This choice of basis ensures that the states of the residual He^+ ion for which $n \leqslant 4$, $\ell \leqslant 3$, are physical, and that any resonances present in the photoionization cross section below the $n = 3$ threshold of He^+ are real, while the inclusion of the additional pseudo-orbitals serves to improve the initial-state wave function. The

basis was generated using a boundary radius of 40.0 a.u. in Eq. (14). As well as improving the initial He ground state, the additional pseudo-orbitals give rise to nonphysical, positive-energy pseudostates, whose inclusion in the expansion of the final-state wave function provides a mechanism for the study of photo-double-ionization. The "bound" photoelectron in the initial state and the ejected photoelectron in the $^1P^o$ final state are described in terms of the same one-electron basis, except that a total of 80 radial functions (or "continuum functions") were included per angular momentum, ℓ, where, in the final state, $\ell = 0, \ldots, 4$. This meant that the same approximation was used in the construction of the R-matrix basis functions in both the initial and final states. The ground-state energy was calculated as -2.8997 a.u. However, by making a small adjustment of -0.0042 a.u. to the diagonal element dominating the calculation of the associated eigenvalue before diagonalization, it was possible to bring the ground-state energy into agreement with the nonrelativistic limit of -2.9037 a.u. reported by Perekis [12].

To estimate the photo-double-ionization cross section we sum the cross section to the positive-energy pseudostates lying above the double-ionization threshold. A correction has been incorporated to account for the contribution from negative-energy pseudostates lying close to threshold, and to eliminate any overestimate from positive-energy pseudostates immediately above threshold. In evaluating the photo-double-ionization cross section we have carried out two calculations. In the energy region from the double-ionization threshold to about 10 eV above this threshold we have extended the R-matrix boundary radius to 70 a.u. in order to increase the density of pseudostates, while at higher energies we have used an R-matrix boundary of 40.0 a.u., which, although giving a less dense pseudo-state basis, spans a much greater energy range. In both calculations we have again used a one-electron orbital basis for the He^+ residual ion consisting of the physical orbitals $1s, 2s, 2p, 3s, 3p, 3d, 4s, 4p, 4d$, and $4f$, augmented by pseudo-orbitals $n = 5$ to $n = 38$, with angular momentum $\ell = 0, \ldots, 3$. We note that the one-electron basis for the higher-energy calculation is the same as that used in the photoionization calculation described above. Both photo-double-ionization calculations included a total of 146 He^+ target states, of which 110 lie above the double-ionization threshold in the first calculation and 120 in the second. Throughout our calculations we have carefully checked convergence with respect to the R-matrix boundary radius, the number and density of pseudostates and the number of radial continuum functions.

B. Results

In Figs. 1 and 2 we present results for photoionization cross sections to the $1s$, $2s$, and $2p$ states of He^+, for photon energies in the region 67.0–72.5 eV. The dominant feature in this energy region is the series of resonances converging onto the He^+ $n = 3$ threshold. In particular, we concentrate on the closed-channel resonance around 70 eV, and compare our results with the recent work of Xu and Shakeshaft [13] and with previous R-matrix calculations of Jiang *et al.* [14]. Our results are generally in good agreement with both these studies, although our data for the $2s$ cross section lie slightly

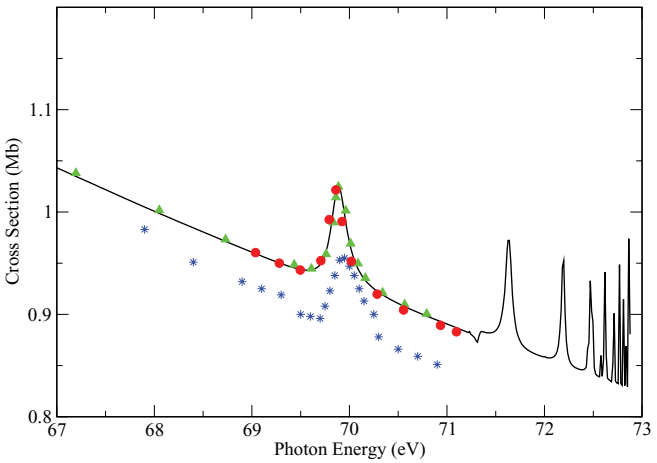

FIG. 1. (Color online) Partial cross section for photoionization of the $^1S^e$ ground state of He to the $1s$ state of He^+. Solid line: present results; triangles: Xu and Shakeshaft [13]; circles: Jiang *et al.* [14]; stars: Lindle *et al.* [15].

higher. In Fig. 1 we have also included the experimental results of Lindle *et al.* [15], which tend to lie about 5% lower than theory. For clarity we have not included the results reported by Jiang *et al.* above 71 eV, but similar agreement is obtained at higher energies.

In Figs. 3 and 4 we give results for the photo-double-ionization calculation by considering the absolute photo-double-ionization cross section and the percentage ratio of double-ionization to single-ionization in the photon energy range 79–130 eV. The results that are presented exhibit small oscillations which are due to the onset of numerous pseudo-state thresholds. These oscillations diminish with increasing pseudostate density and can be removed by a number of techniques, including T-matrix averaging (see, e.g., Burke *et al.* [16]) and box averaging (see, e.g., Bartschat and Bray [17]). Alternatively, when the oscillations are very small, smoothing of the cross section using a Chebyshev series least-squares procedure will suffice. We compare our results

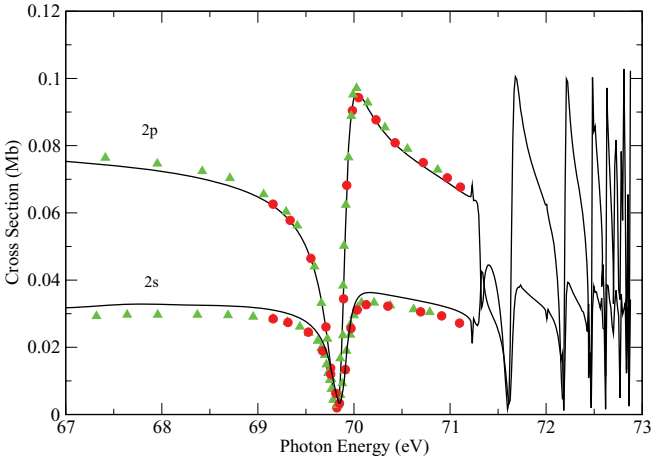

FIG. 2. (Color online) Partial cross section for photoionization of the $^1S^e$ ground state of He to the $2s$ and $2p$ states of He^+. Solid line: present results; triangles: Xu and Shakeshaft [13]; circles: Jiang *et al.* [14].

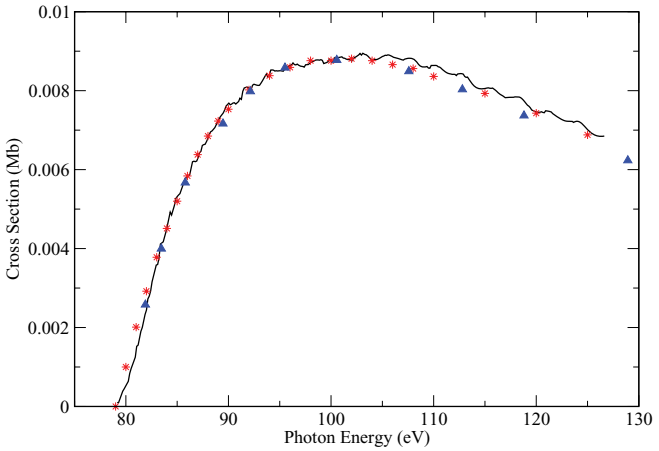

FIG. 3. (Color online) Photo-double-ionization cross section of He. Solid line: present results (unsmoothed); stars: Samson *et al.* [18]; triangles: Ludlow *et al.* [19].

with the experimental data of Samson *et al.* [18] and with the time-dependent close-coupling calculations of Ludlow *et al.* [19] and the convergent close-coupling (CCC) data of Kheifets and Bray [20]. Our evaluations are seen to be in excellent agreement with theory and experiment for both observables.

IV. PHOTODETACHMENT AND PHOTO-DOUBLE-DETACHMENT OF H^-

A. Calculation

We first consider photodetachment of the $^1S^e$ ground state of H^-, leaving the H atom in the state $n\ell$, where $n \leqslant 5$ and $\ell \leqslant 4$, as permitted. Due to the degeneracy of the atomic H energy levels for a particular n, $E_{n\ell}$, $(\ell = 0, \ldots, n-1)$, angular momentum exchange effects exist between the H^- electrons, even out to extremely large distances. For this reason, we have extended the R-matrix radius to 350 a.u., to accurately describe some of the resonance features present in the low

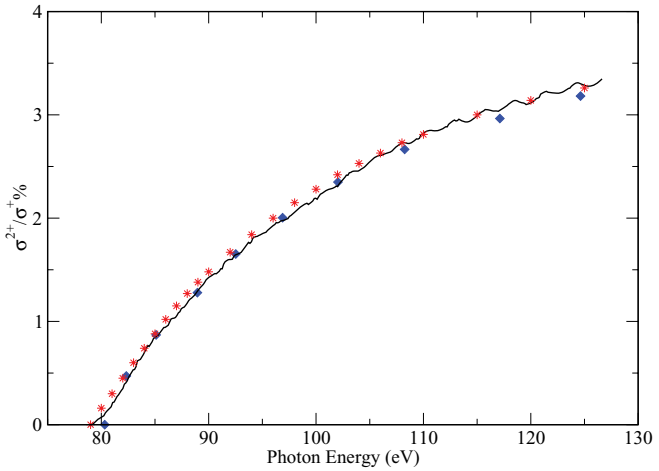

FIG. 4. (Color online) Percentage ratio of double ionization to single ionization in the photoionization of He. Solid line: present results (unsmoothed); stars: Samson *et al.* [18]; diamonds: Kheifets and Bray [20].

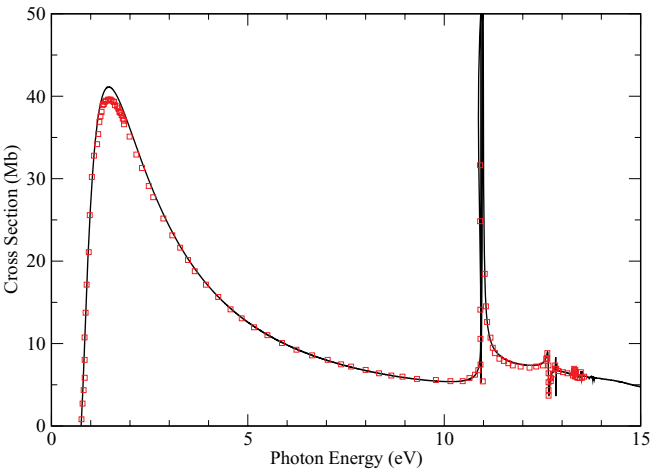

FIG. 5. (Color online) Total photodetachment cross section of H^- up to the $n = 5$ threshold of H. Solid line: present results; squares: Miyake *et al.* [23].

energy region. Physical H orbitals for $n \leqslant 5$, $\ell \leqslant 4$ were included in the construction of the initial- and final-state wave functions, and 200 radial functions were included per angular momentum, ℓ, to describe the "bound" photoelectron in the initial state and the ejected photoelectron in the $^1P^o$ final state. Again this meant that the same approximation was used in the formation of the R-matrix basis functions in both the initial and final states. The ground-state energy of H^- was calculated as $-0.523\,136$ a.u., but this was brought into agreement with the highly accurate nonrelativistic energy of $-0.527\,751$ a.u., calculated by Drake [21], by making an adjustment of $-0.008\,12$ a.u. to the appropriate diagonal element of the two-electron Hamiltonian matrix prior to diagonalization, as described earlier.

B. Results

In Fig. 5 we give an overview of our results for the total cross section for photodetachment of H^- in the photon energy range 0–14 eV, i.e., to just above the H $n = 5$ threshold. Our

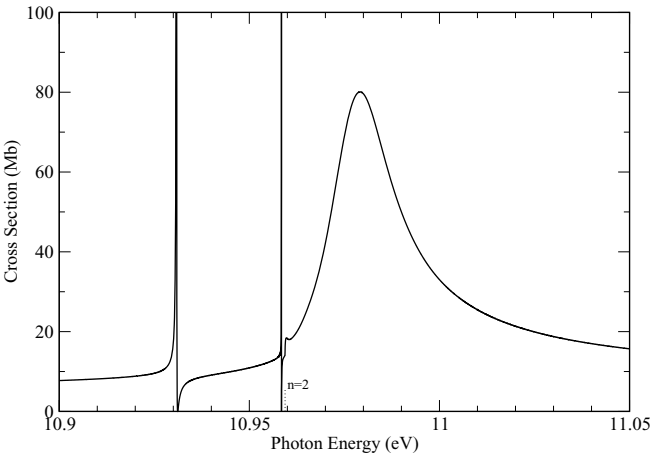

FIG. 6. Total photodetachment cross section of H^- near the $n = 2$ threshold of H.

results are compared with the recent results reported by Miyake *et al*. [23], where a hybrid approach has been adopted which combines R-matrix calculations with high-resolution cross section measurements and previous theoretical results. We note that our *ab initio* data are generally in good agreement with these data throughout the energy region considered, except for the height of the peak at around 2 eV, where the current results lie slightly lower.

In Figs. 6 and 7 we show the total photodetachment cross section in the energy region around the $n = 2$ and $n = 3$ thresholds of H. These energy regions are dominated by shape and closed-channel Feshbach resonances: Detailed results for the width Γ and position E_r of these structures are given in Tables I and II. Γ and E_r have been obtained by fitting the eigenphase sum δ_S to the form

$$\delta_S = \delta_0 + \delta_1 E + \delta_2 E^2 + \arctan\left(\frac{\Gamma}{E_r - E}\right), \qquad (33)$$

where E is the energy of the photoelectron. In Tables I and II we give the resonance position in terms of the total energy $E_{\rm tot}$ of the residual H atom in atomic units, while the width Γ is presented in eV.

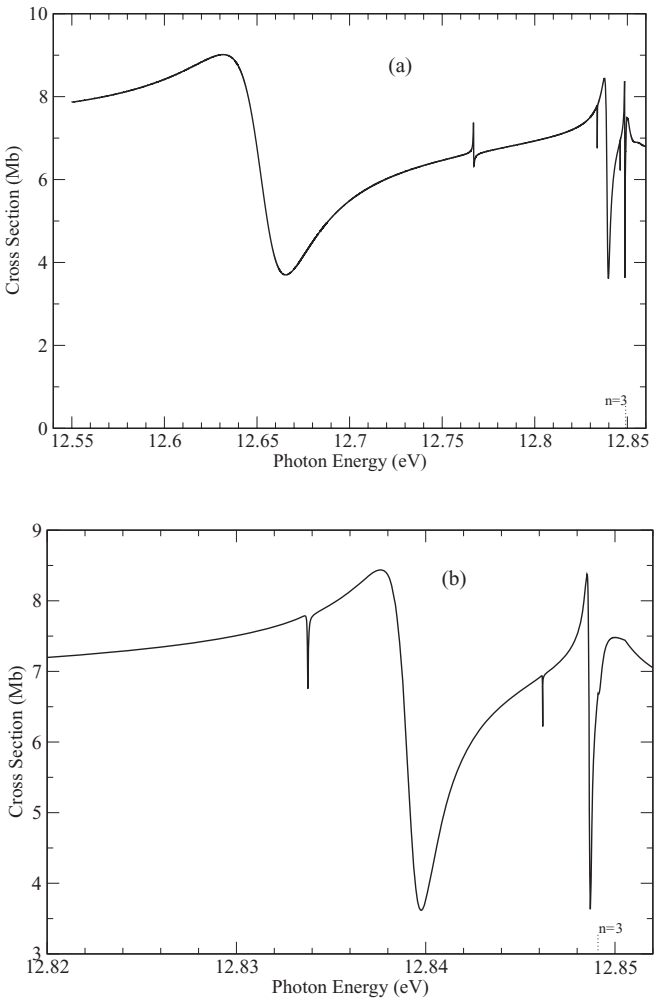

FIG. 7. Total photodetachment cross section of H^- near the $n = 3$ threshold of H. The region close to threshold is shown in more detail in (b).

TABLE I. Theoretical comparison of widths and positions of resonances in the photodetachment cross section of H^- near the $n = 2$ threshold of H.

Source	$E_{\rm tot}$(a.u.)	Γ(eV)
Present	−0.126 05	0.000 038 9
Lindroth[a]	−0.126 05	0.000 034
Sadeghpour *et al*.[b]	−0.126 014	0.000 028 8
Tang *et al*.[c]	−0.126 06	0.000 065
Ho[d]	−0.126 049 8	0.000 035 9
Present	−0.125 03	0.000 000 24
Lindroth	−0.125 04	<0.000 000 2
Tang *et al*.	−0.125 03	
Present	−0.124 50	0.0167
Lindroth	−0.124 37	0.0185
Sadeghpour *et al*.	−0.124 242	0.0186
Tang *et al*.	−0.124 32	0.0169
Ho and Bhatia[e]	$-0.124\,36 \pm 3 \times 10^{-5}$	$0.0188 \pm 2 \times 10^{-4}$

[a]Reference [22].
[b]Reference [24].
[c]Reference [25].
[d]Reference [26].
[e]Reference [27].

We compare our results with those of Lindroth [22], Sadeghpour *et al*. [24], Tang *et al*. [25], Ho [26], and Ho and Bhatia [27]. Lindroth carried out an extremely accurate and

TABLE II. Theoretical comparison of widths and positions of resonances in the photodetachment cross section of H^- near the $n = 3$ threshold of H.

Source	$E_{\rm tot}$(a.u.)	Γ(eV)
Present	−0.062 71	0.0322
Lindroth[a]	−0.062 73	0.0326
Sadeghpour *et al*.[b]	−0.062 695	0.0334
Tang *et al*.[c]	−0.062 72	0.0326
Ho[d]	−0.062 716 75	0.032 40
Present	−0.058 57	0.000 24
Lindroth	−0.058 57	0.000 24
Sadeghpour	−0.058 866	0.000 402
Tang *et al*.	−0.058 59	0.000 261
Ho	−0.058 571 8	0.000 244 4
Present	−0.056 12	0.000 054
Lindroth	−0.056 12	0.000 06
Tang *et al*.	−0.056 14	
Ho	−0.056 116 7	0.000 057
Present	−0.055 92	0.001 83
Lindroth	−0.055 90	0.001 93
Sadeghpour	−0.055 832	0.001 16
Tang *et al*.	−0.055 91	0.001 55
Ho	−0.055 907	0.0019
Present	−0.055 66	0.000 009
Lindroth	−0.055 66	0.000 01
Present	−0.055 57	0.000 14
Lindroth	−0.055 58	0.0001

[a]Reference [22].
[b]Reference [24].
[c]Reference [25].
[d]Reference [26].

detailed study of the photodetachment of H^-, using a complex rotation approach in combination with a discrete numerical basis to form highly correlated descriptions of both the initial and final states. Sadeghpour *et al*. have performed an extensive eigenchannel R-matrix calculation, while the data of Tang *et al*. were obtained using a hyperspherical close-coupling approach. The work of Ho and Ho and Bhatia employed Hylleraas wave functions with the use of complex rotation. Hylleraas wave functions afford a very accurate treatment of correlation effects.

In Fig. 6 we observe three distinct resonances. The first resonance is associated with a doubly excited state dominated by the configurations $2snp$ and $2pns$, while the second extremely narrow resonance is due to a Rydberg-type state. The broad shape resonance just above the $n = 2$ threshold is dominated by configurations of the form $2snp$, $2pns$, and $2pnd$, and has been the subject of detailed study by various theoretical methods. In particular, the height of the peak was investigated by Tang *et al*., who concluded that this value was related to the accuracy of the initial-state wave function for H^-. They reported a value of 78.6 Mb for the approximation, which they considered to be most accurate. The height of this peak from the current work is 80.09 Mb, while Lindroth reports a value of 76 Mb. We see from Table I that our results are in excellent agreement with the other theoretical results tabulated.

In Fig. 7 the first two resonances are dominated by configurations of the form $n_1\ell_1 n_2\ell_2$, where $n_1 = n_2 = 3$ and $n_1 = 3, n_2 = 4$. The remaining resonances are associated with Rydberg-type states. In Table II we compare the width and positions of the resonances in this energy region with other theoretical data. We again see that the present results are in excellent agreement with previous calculations.

Finally, we consider photo-double-detachment of H^-. We illustrate results for this process in Fig. 8 where we compare data for the percentage ratio for double detachment to single detachment with CCC results of Kheifets and Bray [20]. In this calculation we have included up to $n = 3$ physical states augmented by an additional 27 pseudostates per angular momentum, and have used an R-matrix boundary of 60 a.u. The calculation has also been repeated with a boundary radius of 70 a.u. and 80 a.u., including 32 and 33 pseudostates per angular momentum, respectively. As these results are in accord with each other, we only present the results from the first model, for which we give both the smoothed and unsmoothed results. We see that the present calculation is in excellent agreement with the work of Kheifets and Bray.

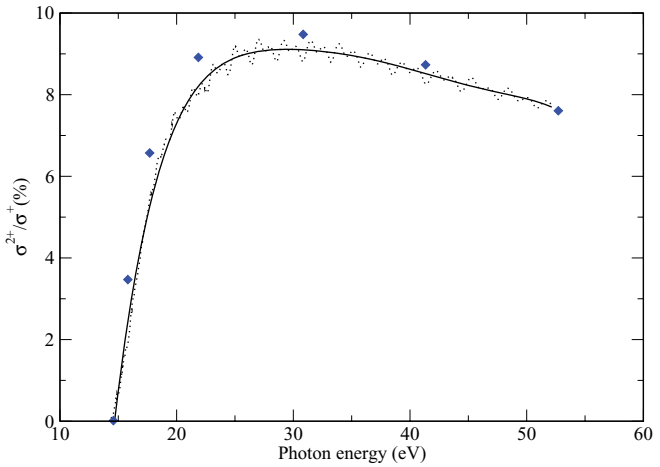

FIG. 8. (Color online) Percentage ratio of double ionization to single ionization in the photodetachment cross section of H^-. Solid line: present results (smoothed); dotted line: present results (unsmoothed); diamonds: Kheifets and Bray [20].

V. CONCLUSIONS

We have developed and implemented the theory for an IERM approach to photoionization which, through the use of suitably constructed pseudostates, allows accurate calculation of both single- and double-ionization processes. This has been demonstrated by the excellent agreement obtained with other highly regarded theoretical methods, such as the CCC method of Kheifets and Bray [20] and the time-dependent close-coupling approach of Ludlow *et al*. [19], and with experiment, e.g., Samson *et al*. [18]. We have been able to describe the two-electron bound initial state and the final state, where either one or two electrons have been ejected, in terms of the same one-electron orbital basis. We are therefore confident that this approach can be successfully incorporated into a many-electron R-matrix approach, either time-dependent or time-independent, where $(N + 2)$-, $(N + 1)$-, and N-electron systems would, similarly, be constructed from a single one-electron orbital basis. As such, it forms a key step in the development of a multipurpose R-matrix code for multiple-electron ejection, which will be capable of generating highly accurate data for time-dependent and time-independent processes in the burgeoning areas of attosecond science and application of advanced x-ray lasers.

The IERM approach for electron collisions with atoms and ions has been extended, by inclusion of a model potential, to consider electron scattering from quasi-one-electron atoms and ions [28]. Similar modifications have been made to the IERM photoionization codes, and photoionization calculations, with double ionization, are currently being carried out on suitable ions of Ne and Ar, such as Ne^{6+}, Ne^{8+}, Ar^{8+}, Ar^{14+}, and Ar^{16+}. We anticipate that data produced will be of interest in the field of attosecond science, as these elements are frequently used as the atomic or ionic target in such experiments. To extend this work further to consider general many-electron atoms and ions, additional theoretical and computational developments are underway which will allow two interacting electrons in the R-matrix external region. The current IERM codes and the recently developed two-dimensional R-matrix propagator program 2DRMP [11] can be used in this region and linked to a modified R-matrix internal region, thus facilitating accurate treatment of double-electron continua within an R-matrix framework [29].

ACKNOWLEDGMENTS

The authors wish to thank Professor H. van der Hart and Professor P. G. Burke for valuable discussions. A.J.K. and M.W.McI. were supported by Northern Ireland DEL postgraduate studentships.

[1] P. B. Corkum and F. Krausz, Nat. Phys. **3**, 281 (2007).
[2] N. Rohinger, D. Ryan, R. A. London, M. Purvis, F. Albert, J. Dunn, J. D. Bozek, C. Bostedt, A. Graf, R. Hill, S. Hau-Riege, and J. Rocca, Nature (London) **481**, 488 (2012).
[3] P. G. Burke and K. T. Taylor, J. Phys. B **8**, 2620 (1975).
[4] M. A. Lysaght, P. G. Burke, and H. W. van der Hart, Phys. Rev. Lett. **101**, 253001 (2008).
[5] L. R. Moore, M. A. Lysaght, J. S. Parker, H. W. van der Hart, and K. T. Taylor, Phys. Rev. A **84**, 061404(R) (2011).
[6] P. G. Burke, C. J. Noble, and M. P. Scott, Proc. R. Soc. Lond. A **410**, 289 (1987).
[7] T. T. Scholz, J. Phys. B **24**, 2127 (1991).
[8] M. P. Scott, T. T. Stitt, N. S. Scott, and P. G. Burke, J. Phys. B **35**, L323 (2002).
[9] O. Zatsarinny and K. Bartschat, Phys. Rev. Lett. **107**, 023203 (2011).
[10] A. C. Brown, S. H. Hutchinson, M. A. Lysaght, and H. W. van der Hart, Phys. Rev. Lett. **108**, 063006 (2012).
[11] N. S. Scott, M. P. Scott, P. G. Burke, T. Stitt, V. Faro-Maza, C. Denis, and A. Maniopoulou, Comput. Phys. Commun. **180**, 2424 (2009).
[12] C. L. Pekeris, Phys. Rev. **126**, 1470 (1963).
[13] H. Xu and R. Shakeshaft, Phys. Rev. A **83**, 012716 (2011).
[14] Y. H. Jiang, R. Püttner, and G. Kaindl, J. Phys. B **38**, 2157 (2005).
[15] D. W. Lindle, T. A. Ferrett, P. A. Heimann, and D. A. Shirley, Phys. Rev. A **36**, 2112 (1987).
[16] P. G. Burke, K. A. Berrington, and C. V. Sukumar, J. Phys. B **14**, 289 (1981).
[17] K. Bartschat and I. Bray, J. Phys. B **29**, L577 (1996).
[18] J. A. R. Samson, W. C. Stolte, Z.-X. He, J. N. Cutler, Y. Lu, and R. J. Bartlett, Phys. Rev. A **57**, 1906 (1998).
[19] J. A. Ludlow, T.-G. Lee, and M. S. Pindzola, Phys. Rev. A **81**, 023407 (2010).
[20] A. S. Kheifets and I. Bray, Phys. Rev. A **58**, 4501 (1998).
[21] G. W. F. Drake, Nucl. Instrum. Methods Phys. Res., Sect. B **31**, 7 (1988).
[22] E. Lindroth, Phys. Rev. A **52**, 2737 (1995).
[23] S. Miyake, P. C. Stancil, H. R. Sadeghpour, A. Dalgarno, B. M. McLaughlin, and R. C. Forrey, Astrophys. J. Lett. **709**, L168 (2010).
[24] H. R. Sadeghpour, C. H. Greene, and M. Cavagnero, Phys. Rev. A **45**, 1587 (1992).
[25] J.-Z. Tang, S. Watanabe, and M. Matsuzawa, Phys. Rev. A **46**, 2437 (1992).
[26] Y. K. Ho, Phys. Rev. A **45**, 148 (1992).
[27] Y. K. Ho and A. K. Bhatia, Phys. Rev. A **48**, 3720 (1993).
[28] A. J. Kinnen, Ph.D. thesis, Queen's University Belfast, 2005.
[29] P. G. Burke, *R-Matrix Theory of Atomic Collisions* (Springer-Verlag, Berlin, 2011).